ELSEVIER

Journal of Power Sources 103 (2002) 188–200

JOURNAL OF POWER SOURCES

www.elsevier.com/locate/jpowsour

Energy and exergy analysis of simple solid-oxide fuel-cell power systems

S.H. Chan*, C.F. Low, O.L. Ding

Fuel-Cell Technology Strategic Research Programme, School of Mechanical and Production Engineering, Nanyang Technological University, 50 Nanyang Avenue, Singapore 639798, Singapore

Received 19 March 2001; accepted 19 June 2001

Abstract

Two, simple, solid-oxide fuel-cell (SOFC) power systems fed by hydrogen and methane, respectively, are examined. While other models available in the literatures focus on complicated hybrid SOFC and gas-turbine (GT) power systems, this study focuses on simple SOFC power systems with detailed thermodynamic modeling of the SOFC. All performance-related parameters of the fuel-cell such as respective resistivity of the components, anode and cathode exchange current density, limiting current density, flow diffusivity, etc. are all expressed as a function of temperature, while the flow through of each nodes of the system is described as a function of thermodynamic state. Full analysis of the energy and exergy at each node of the system is conducted and their respective values are normalized by the lower heating value (LHV) of the fuel and its chemical exergy, respectively. Thus, the normalized electrical energy outputs directly indicate the first law and second law efficiencies, respectively, of the fuel-cell power systems.

Keywords: Exergy; Solid-oxide fuel-cell; First and second law efficiencies; Fuel utilization; Hydrogen; Methane

1. Introduction

If one can still recall the Kyoto conference in December 1997 that highlighted the disparate energy usage needs and aspirations of many countries, he/she would have no question on the imperative for clean and efficient use of energy within all countries. It is also recognized, in both established and fast growing economies, that the legitimate desire to maintain or improve the quality of life should be consistent with the responsible use of energy. Responsible usage of energy corresponds to efficient use of energy and minimum impact to the global environment. To meet the requirements of the Kyoto Protocol, the fuel-cell as an emerging technology has been considered to be a potential candidate to replace conventional internal combustion engines for propulsion and to integrate with gas-turbine (GT) technology for power generation.

In power generation, because of the synergistic effects of integrated solid-oxide fuel-cell (SOFC) and GT technologies, predicted results have shown [1,2] that an overall system efficiency of 70% (net ac/lower heating value (LHV)) or higher is possible with a more complex thermodynamic cycle. These studies were based mainly on the analysis of the thermodynamic system using first law of thermodynamics in conjunction with a techno-economical assessment. On other hand, increasingly more researchers are applying the second law of thermodynamics to the analysis of the overall plant efficiency by calculating the exergy content at each node of the thermodynamic system and the respective energy destruction in each system component [3,4]. Knowing the extent of the losses distribution in the thermodynamic system, attention can be focused on improvements in a particular system component or process. A detailed description of exergy analysis and the reduction of irreversibility has been given by Cornelissen [5]. This study also provided a basis for the relationship between exergy analysis and environmental life-cycle analysis (LCA).

In this paper, we present two simple SOFC power systems fed by hydrogen (H_2) and methane (CH_4), respectively. A simulation technique is applied and individual system component models are developed and integrated in the simulation code. Emphasis is placed on the development of a more complete SOFC model, which can be used to simulate different designs of SOFC provided that the geometric specifications, performance-related parameters and operating conditions are specified. The study also provides the foundation for future analysis of a more complex power system.

* Corresponding author. Tel.: +65-790-4862; fax: +65-791-1859.
E-mail address: mshchan@ntu.edu.sg (S.H. Chan).

0378-7753/02/$ – see front matter
PII: S0378-7753(01)00842-4

Nomenclature

a	coefficient
C	concentration
e	energy of molecular interaction
E	voltage
Ex	exergy
F	Faraday constant
g	acceleration due to gravity
H	enthalpy
i	current density
i_o	exchange current density
i_{oa}	anode exchange current density
i_{oc}	cathode exchange current density
I	current
l	distance
l_a	distance from anode surface to reaction sites
l_c	distance from cathode surface to reaction sites
M	molecular mass
n	mole number
p	pressure
Q	heat
R	universal gas constant
S	entropy
T	temperature
V	velocity
W	work done

Greek letters

η	polarization
η_{Act}	activation polarization
η_{Conc}	concentration polarization
η_{Ohm}	Ohmic polarization
ρ	resistivity
σ	collision diameter
σ_{cv}	entropy production
Ω_D	collision integral based on the Lennard–Jones potential
ξ	tortuosity

2. Exergy

2.1. Exergy concept

Exergy is defined as the maximum obtainable work a substance can yield when it is brought reversibly to equilibrium with the environment. The exergy method of analysis is essentially based on the second law of thermodynamics and the concept of irreversible entropy production. It is concerned with the efficiency of use of the available work that is generated from energy resources, and therefore, enables determination of the location, type and *true* magnitude of each loss in a thermodynamic system. Such information is useful when designing a thermal system or reducing sources of inefficiency in an existing system.

The environment is generally the surrounding environment of the system since the final deposition of the initially available energy will be through external cooling devices or ejection of an energy-bearing substance into the environment. It is a very large *reservoir* in the state of perfect thermodynamic equilibrium, in which no gradients of pressure, temperature, chemical potential, kinetic or potential energy can exist. Thus, there is no possibility of producing work from any form of interaction between parts of the environment. The environment, therefore, is a natural reference for assessing the work potential of different kinds of systems.

Three forms of exergy transfer are usually established to perform an exergy analysis of a system, namely, exergy transfer with work interaction, heat interaction and material streams. Other forms of exergy transfer include friction, momentum, potential interaction, etc.

In conducting exergy analysis, two forms of equilibrium, the environmental state and the dead state are considered. The environmental state is a restricted equilibrium where the conditions of mechanical (p) and thermal (T) equilibrium are satisfied. The dead state is an unrestricted equilibrium where the conditions of mechanical (p), thermal (T) and chemical (μ) equilibrium are satisfied. Under this full thermodynamic equilibrium between the system and the environment, the system cannot undergo any changes of state through any form of interaction with the environment.

The control volume of a thermodynamic system with a single inlet and outlets is shown in Fig. 1. The exergy of this system can be express as:

$$\sum\left(1-\frac{T_o}{T_j}\right)\dot{Q}_{cv}-\dot{W}_{cv}+\dot{m}\left[(h_1-h_2)-T_o(S_1-S_2)+\frac{V_1^2-V_2^2}{2}+g(z_1-z_2)\right]-\sigma_{cv}=0 \quad (1)$$

For each component process, an exergy balance can be established. By considering all the in-going and out-going exergy flows, the exergy destruction can be calculated. When dealing with the exergy of a process component, the difference between exergy losses and destruction should

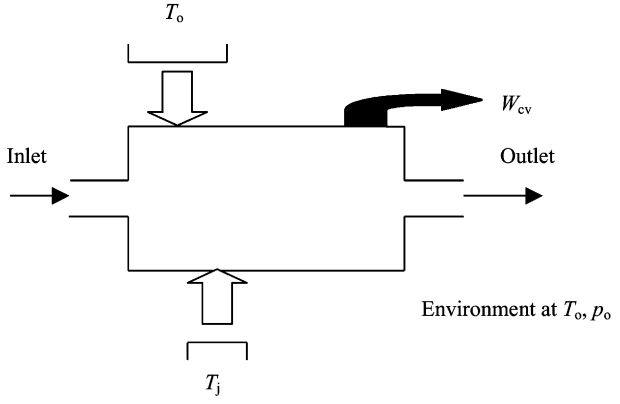

Fig. 1. An open thermodynamic system with a single inlet and outlet.

be noted. Exergy losses consist of exergy flowing to the surroundings, whereas, exergy destruction indicates the loss of exergy within the system boundary due to irreversibility.

2.2. Exergy components

In calculating the exergy of a stream of matter, the exergy can be divided distinctively into different components. In the absence of nuclear effects, magnetism, electricity and surface tension:

$$\mathrm{Ex} = E_\mathrm{k} + E_\mathrm{p} + E_\mathrm{phy} + E_\mathrm{chem} \quad (2)$$

where E_k, E_p, E_phy, and E_chem are kinetic exergy, potential exergy, physical exergy and chemical exergy, respectively.

In this study, only physical and chemical exergies are considered at different nodes of the system, while kinetic and potential effects are neglected. Physical exergy is defined as the maximum amount of work obtainable when the stream of substance is brought from its initial state to the environmental state defined by p_o and T_o, by physical processes which involve only thermal interaction with the environment. Chemical exergy is defined as the maximum amount of work obtainable when the substance is brought from the environmental state to the dead state by processes involving heat transfer and exchange of substance only with the environment.

3. Modeling

The simulation program developed consists of two mathematical models, namely, the electrochemical model and the heat exchanger model for fuel-cell systems operating on hydrogen or methane. A H_2-fed SOFC system, which incorporates two pre-heaters, a SOFC stack and an afterburner, is shown in Fig. 2. The slightly more complex CH_4-fed SOFC system, as shown in Fig. 3, incorporates a mixer, a vaporizer, two pre-heaters, an external reformer, a SOFC stack, and an afterburner. The reformer used is a steam-reforming type, which requires an external heat source for the endothermic reaction. The reformer reforms the CH_4 to H_2-rich reformate following the chemical reaction:

$$\mathrm{CH_4} + 2.444\mathrm{H_2O} \rightarrow \mathrm{CO_2} + 4\mathrm{H_2} + 0.444\mathrm{H_2O} \quad (3)$$

The minimum mole number of water vapor required for steam reforming is two. The additional 0.444 moles of water vapor are used to prevent possible thermal decomposition of the methane that would otherwise form solid carbon which would deactivate the catalytic reaction of the reformer.

The simulation program, written in Visual Basic, allows the user to specify the operating pressures, fuel supplying rate, fuel utilization rate, percentage of theoretical airflow, reformer efficiency and temperatures at certain points of the system. After accepting the user's entry data, it performs a calculation to determine the molar chemical compositions of the flow streams at different nodes of the system and the amount of air required by the SOFC stack and afterburner to sustain the system operation. Then, it calls on the electrochemical model to determine the electrical work output of the SOFC stack, its associated heat rejection to the surroundings, and the exit flow temperature. Following this, the heat exchanger model is called to determine the exit temperatures of the two pre-heaters. Based on these calculated temperatures, the enthalpy and exergy at corresponding points can be determined. These enthalpies and exergies are then normalized relative to the LHV and chemical exergy of the fuel, respectively.

The physical and chemical exergies are calculated using the following equation:

$$E_\mathrm{phy} = E_\mathrm{chem} = (H_n - H^\circ) - T_\mathrm{o}(S_n - S^\circ) \quad (4)$$

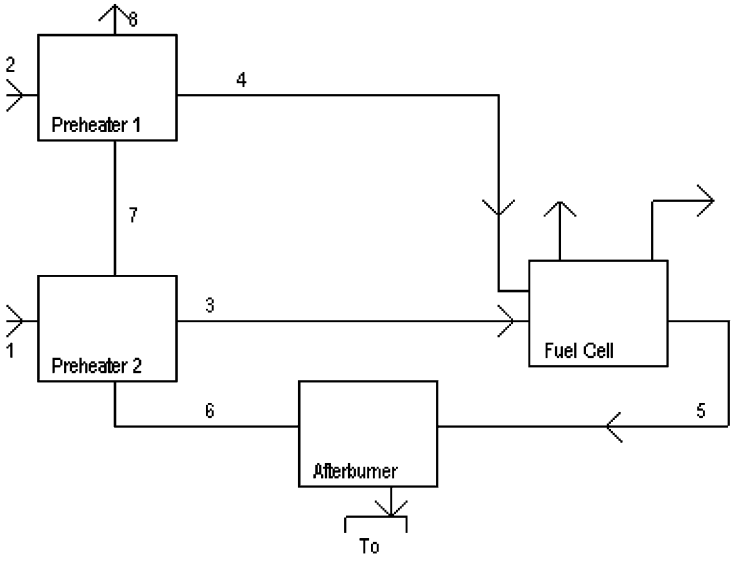

Fig. 2. Hydrogen-fed fuel-cell system.

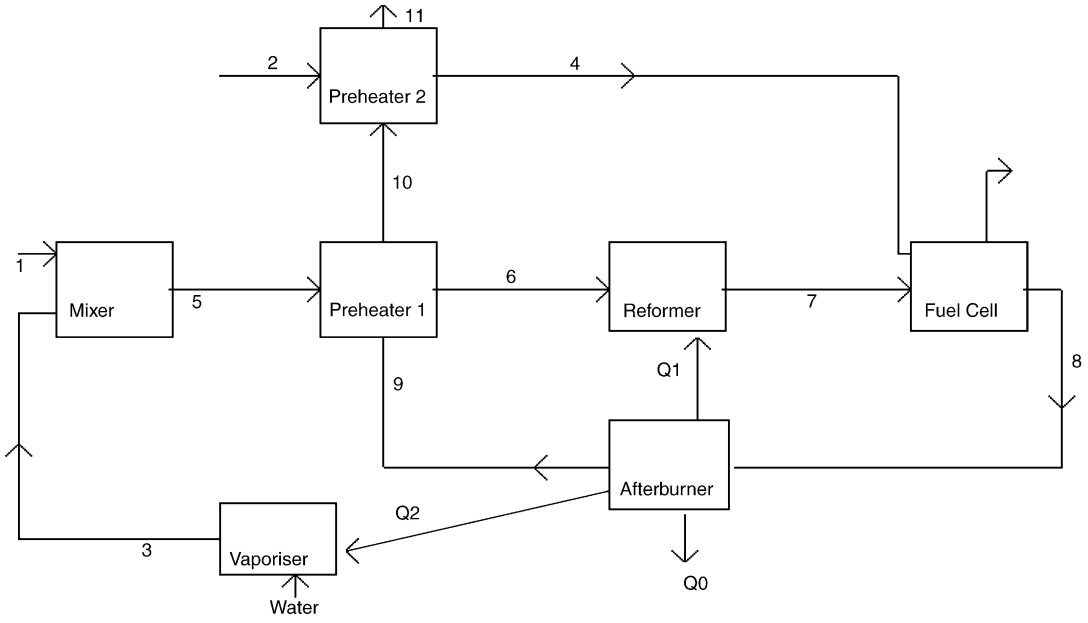

Fig. 3. Methane-fed fuel-cell system.

where subscript n refers to the state points of a system, $^\circ$ refers to environmental condition, H is the enthalpy, and S the entropy.

Assuming that the gases obey ideal gas behavior, their respective enthalpies and entropies can be determined from the following polynomial equations fitted to the data of the JANAF table [6].

$$\frac{H^\circ}{RT} = a_1 + \frac{a_2}{2}T + \frac{a_3}{3}T^2 + \frac{a_4}{4}T^3 + \frac{a_5}{5}T^4 + \frac{a_6}{T} \quad (5)$$

$$\frac{S^\circ}{R} = a_1 \ln(T) + a_2 T + \frac{a_3}{2}T^2 + \frac{a_4}{3}T^3 + \frac{a_5}{4}T^4 + a_7 \quad (6)$$

The coefficients, a_1–a_7, for different gases used in this study can be found in Table 1.

The assumptions and conditions of model used in the simulation program are listed as follows:

- steady flow with negligible frictional losses;
- negligible changes of potential and kinetic energies in any processes;
- the environment is at STP conditions, i.e. 298 K and 1 atm;
- isothermal process in the afterburner;
- all other gases except hydrogen and oxygen are considered to be diluents;
- wet atmospheric air is used;
- stoichiometric fuel–air reaction throughout;
- default fuel supplying rate is 1 kg s^{-1}.

3.1. Electrochemical model

The electrochemical model considers the effect of all forms of overpotential on the SOFC performance, its associated heat lost, and the electrical energy produced. Since all the performance related parameters are dependent on temperature, iterations are performed to calculate the stack temperature, with known thermodynamic state at the inlets of the fuel-cell, until convergence criteria is met.

3.1.1. Activation overpotential

To avoid the ambiguity of simplified models, such as the Tafel equation or a linear potential–current relation, used under different operating conditions, the following general Butler–Volmer equation is used to calculate the respective overpotential of the anode and cathode:

$$i = i_o \left\{ \exp\left(\beta \frac{n_e F \eta_{Act}}{RT}\right) - \exp\left[-(1-\beta)\frac{n_e F \eta_{Act}}{RT}\right] \right\} \quad (7)$$

where β is the transfer coefficient and i_o the 'apparent' exchange current density. The transfer coefficient is considered to be the fraction of the change in polarization that leads to a change in the reaction rate constant; its value is usually 0.5 in the context of a fuel-cell. Hence,

$$i = 2i_o \sinh\left(\frac{n_e F \eta_{Act}}{2RT}\right) \quad (8)$$

or

$$\eta_{Act} = \frac{2RT}{n_e F} \sinh^{-1}\left(\frac{i}{2i_o}\right) \quad (9)$$

The 'apparent' exchange current density is a function of temperature, which is related to the charge transfer resistance by:

$$r_{ct} = \frac{RT}{nFi_o} \quad (10)$$

or

$$i_o = \frac{RT}{nFr_{ct}} \quad (11)$$

Table 1
Coefficients used in Eqs. (5) and (6) for various gases[a]

Species	Coefficients						
	a_1	a_2	a_3	a_4	a_5	a_6	a_7
300 K < T < 1000 K							
Ar	2.50000000E+00	0.00000000E+00	0.00000000E+00	0.00000000E+00	0.00000000E+00	−7.45375020E+02	4.36600060E+00
CH_4	1.50270720E+00	1.04167980E−02	−3.91815220E−06	6.77778990E−10	−4.42837060E−14	−9.97870780E+03	1.07071430E+01
CO_2	4.46080410E+00	3.09817190E−03	−1.23925710E−06	2.27413250E−10	−1.55259540E−14	−4.89614420E+04	−9.86359820E−01
H_2	3.10019010E+00	5.11194640E−04	5.26442100E−08	−3.49099730E−11	3.69453450E−15	−8.77380420E+02	−1.96294210E+00
H_2O (G)	2.71676330E+00	2.94513740E−03	−8.02243740E−07	1.02266820E−10	−4.84721450E−15	−2.99058260E+04	6.63056710E+00
H_2O (L)	1.27127820E+01	−1.76627900E−02	−2.25566610E−05	2.08209080E−07	−2.40786140E−10	−3.74832000E+04	−5.91153450E+01
N_2	2.89631940E+00	1.51548660E−03	−5.72352770E−07	9.98073930E−11	−6.52235550E−15	−9.05861840E+02	6.16151480E+00
O_2	3.62195350E+00	7.36182640E−04	−1.96522280E−07	3.620155880E−11	−2.89456270E−15	−1.20198250E+03	3.61509600E+00
5000 K < T < 1000 K							
Ar	2.50000000E+00	0.00000000E+00	0.00000000E+00	0.00000000E+00	0.00000000E+00	−7.45374980E+02	4.36600060E+00
CH_4	3.82619320E+00	−3.97945810E−03	2.45583400E−05	−2.27329260E−08	6.96269570E−12	−1.01449500E+04	8.66900730E−01
CO_2	2.40077970E+00	8.73509570E−03	−6.60708780E−06	2.00218610E−09	6.32740390E−16	−4.83775270E+04	9.69514570E+00
H_2	3.05744510E+00	2.67652000E−03	−5.80991620E−06	5.52103910E−09	−1.81227390E−12	−9.88904740E+02	−2.29970560E+00
H_2O (G)	4.07012750E+00	−1.10844990E−03	4.15211800E−06	−2.96374040E−09	8.07021030E−13	−3.02797220E+04	−3.22700460E−01
H_2O (L)	1.27127820E+01	−1.76627900E−02	−2.25566610E−05	2.08209080E−07	−2.40786140E−10	−3.74832000E+04	−5.91153450E+01
N_2	3.67482610E+00	−1.20815000E−03	2.32401020E−06	−6.32175590E−10	−2.25772530E−13	−1.06115880E+03	2.35804240E+00
O_2	3.62559850E+00	−1.87821840E−03	7.05545440E−06	−6.76351370E−09	2.15559930E−12	−1.04752260E+03	4.30527780E+00

[a] JANAF table.

where

$$i_o = A e^{-(B/RT)} \tag{12}$$

3.1.2. Ohmic overpotential

Ohmic overpotential, which contributes by the electrolyte, electrodes and interconnector of the fuel-cell, occurs because of the resistance to the flow of ions in the ionic conductors and the resistance to electrons through the electronic conductors. Since these resistances obey Ohm's law, the overall Ohmic overpotential can be written as:

$$\eta_{Ohm} = iR \tag{13}$$

The resistance of each material used in the SOFC components can be calculated from its respective resistivity, which is a function of temperature [7], i.e.

$$R = \frac{\rho\delta}{A} \tag{14}$$

and

$$\rho = a e^{(b/T)} \tag{15}$$

where a and b are the constants which are specific to the materials.

3.1.3. Concentration overpotential

To avoid a heavily reliance on correlation to determine the limiting current density, the complete concentration overpotential equations derived in a previous study can be used [8], namely:

$$\text{anode}: \quad \eta_{Conc,a} = -\frac{RT}{2F} \ln\left[\frac{1-(RT/2F)(l_a/D_{eff,a}p^I_{H_2})i}{1+(RT/2F)(l_a/D_{eff,a}p^I_{H_2O})i}\right] \tag{16}$$

$$\text{cathode}: \quad \eta_{Conc,c} = -\frac{RT}{2F} \ln\left[\frac{(p_c/\delta_{O_2} - (p_c/\delta_{O_2} - p_{O_2})\exp(RT/4F(\delta_{O_2}l_c/D_{eff,c}p_c)i))}{P^I_{O_2}}\right] \tag{17}$$

Concentration overpotential becomes significant when large amounts of current are drawn from the fuel-cell. The partial pressures of the gases at the reaction sites, which corresponds to the volume concentrations of the gases, will be less than that in the bulk of the gas stream when a large amount of current is drawn. If such partial pressures or concentrations of gases are unsustainable, concentration polarization will cause excessive voltage losses and the fuel-cell will cease to operate.

Diffusion through a porous media can be described by either ordinary or Knudsen diffusion. In this context, both types of diffusion are included in the model to render it more generalized. Ordinary diffusion occurs when the pore diameter of the porous material is large in comparison with the mean free path of the gas molecules, whereas, for Knudsen diffusion, molecular transport is through pores which are small in comparison to the mean free path of the gas. In Knudsen diffusion, molecules collide more frequently with the pore walls than with other molecules. Upon collision, the atoms are instantly adsorbed on to the surface and are then desorbed in a diffused manner. As a result of frequent collisions with the wall of the pore, the transport of the molecules is impeded.

In the Knudsen diffusion, the diffusion coefficient for straight and round pores is expressed by [9]:

$$D_K = 97r\sqrt{\frac{T}{M_A}} \tag{18}$$

To account for the tortuous path of the gas molecules rather than travel along the radial direction, and for the porosity of the ceramic given that diffusion occurs only in the pore space, an effective Knudsen diffusion coefficient is defined:

$$D_{K,eff} = D_K\frac{\varepsilon}{\xi} \tag{19}$$

Using the Chapman–Enskog theory of prediction, the binary ordinary diffusion coefficient in the gas phase can be calculated by [10]:

$$D_B = 1.8583\times10^{-7}\left(\frac{1}{M_A}+\frac{1}{M_B}\right)^{1/2}\frac{T^{3/2}}{p\sigma^2_{AB}\Omega_{D,AB}} \tag{20}$$

where p is the total pressure in atm; $\sigma_{AB} = (\sigma_A + \sigma_B)/2$ the collision diameter in angstroms (Å); $\Omega_{D,AB}$ the collision integral based on the Lennard–Jones potential and can be obtained from e_{AB} which is the energy of molecular interaction in ergs ($e_{AB}/k = \sqrt{(e_A/k)(e_B/k)}$).

Similar to Knudsen diffusion, the effective diffusion coefficient for ordinary diffusion is defined as:

$$D_{AB,eff} = D_{AB}\frac{\varepsilon}{\xi} \tag{21}$$

To account for the combined effect of Knudsen and ordinary diffusion in the diffusion process, a combined diffusion coefficient is used, i.e.

$$\frac{1}{D_{A,eff}} = \frac{1}{D_{AB,eff}} + \frac{1}{D_{AK,eff}} \tag{22}$$

3.1.4. Electrical power and heat transfer losses

Once all the overpotentials are computed, the cell voltage can be determined by subtracting these overpotentials from the Nernst potential:

$$E(i) = E_o - (\eta_{Ohm} + \eta_{Act,a} + \eta_{Act,c} + \eta_{Conc,a} + \eta_{Conc,c}) \tag{23}$$

where the Nernst potential is given by:

$$E_o = \frac{RT}{2F}\ln K - \frac{RT}{4F}\ln\left(\frac{p^2_{H_2O}}{(p^I_{H_2})^2 p^I_{O_2}}\right) \tag{24}$$

Table 2
Conditions of heat exchanger[a]

Type of fuel	Pre-heater no.	Inlet temperature cold side (K)	Outlet temperature cold side (K)	Inlet temperature hot side (K)	Outlet temperature hot side (K)	Calculated pre-heater size (m^2) (include fouling factor)
Hydrogen	2	298	1100	1200	1157	650
	1	298	1117	1157	382	63400
Methane	2	298	1140	1200	1143	550
	1	298	1102	1143	412	26300

[a] Operating conditions: fuel flow rate, 1 kg s^{-1}; air flow rate, 600%; theoretical air, 1 atm (both anode and cathode); fuel utilization rate, 75%; reformer efficiency, 90% (methane-fed system only); overall heat transfer coefficient, 0.05 kW m^{-2} K.

The electrical power density produced by the fuel-cell is calculated by:

$$W = EI \tag{25}$$

Similarly, the heat lost to the environment at an equilibrium state can be determined readily by evaluating the entropy rate balance for a control volume, i.e.

$$Q_{cv} = T(\Delta S - \sigma_{cv}) \tag{26}$$

where

$$\Delta S = \left(S^{\circ}_{H_2O} - S^{\circ}_{H_2} - \frac{1}{2} S^{\circ}_{O_2} \right) + \frac{R}{2} \ln \left(\frac{(p^{I}_{H_2})^2 p_{O_2}}{(p^{I}_{H_2O})^2} \right) \tag{27}$$

The 'thermodynamic' entropy production, which is actually the irreversibility, is related to the 'electrochemical' overpotential as:

$$\sigma_{cv} = \frac{2F}{T} (\eta_{Ohm} + \eta_{Act,a} + \eta_{Act,c} + \eta_{Conc,a} + \eta_{Conc,c}) \tag{28}$$

3.2. Heat exchanger model

3.2.1. Design of heat exchanger

The effectiveness-number of transfer units (ε-NTU) method is used to model the pre-heaters in H_2- and CH_4-fed fuel-cell systems [11]. In this study, counter-flow types of heat exchanger are selected as the pre-heaters, and are sized according to the following prescribed conditions given in Table 2.

3.2.2. Performance calculation

The simulation code is designed to allow the users to vary the inlet and operating conditions of the system. To determine the outlet temperatures of the pre-heaters, which vary with the inlet conditions, the heat capacity rates of the cold and hot gas streams are calculated:

$$C_c = \sum \dot{n}_c c_{p,c} \tag{29}$$

$$C_h = \sum \dot{n}_h c_{p,h} \tag{30}$$

By comparing their values, the lower and higher values are assigned as C_{min} and C_{max}, respectively. The ratio of heat capacity rates is then available. Thus,

$$C_r = \frac{C_{min}}{C_{max}} \tag{31}$$

The effectiveness of cross-flow heat exchangers can be calculated from:

$$\varepsilon = \frac{1 - e^{[-NTU(1-C_r)]}}{1 - C_r e^{[-NTU(1-C_r)]}}, \quad \text{for } C_r < 1 \tag{32}$$

$$\varepsilon = \frac{NTU}{1 + NTU}, \quad \text{for } C_r = 1 \tag{33}$$

where

$$NTU = \frac{UA}{C_{min}} \tag{34}$$

Hence, the heat exchange rate between the hot and the cold gas streams is:

$$q = \varepsilon q_{max} \tag{35}$$

where the theoretical maximum heat transfer rate is

$$q_{max} = C_{min}(T_{h,i} - T_{c,i}) \tag{36}$$

Based on the energy balance, the exit temperatures of the hot and cold gas streams from the heat exchanger are:

$$T_{h,o} = T_{h,i} - \frac{q}{C_h} \tag{37}$$

$$T_{c,o} = T_{c,i} + \frac{q}{C_c} \tag{38}$$

Since the inlet temperatures of the heat exchangers are affected by the exit flow temperature of the SOFC stack, the above procedures are repeated until the exit temperatures of the pre-heaters converge.

4. Results and discussions

Details of various overpotentials as a function of current density in a fuel-cell operated at 800°C are shown in Fig. 4. The limiting current density at this operating temperature is 2980 A m^{-2}. Results show that cathode activation and Ohmic overpotentials are responsible for the major losses in the fuel-cell over the normal operating range. The cathode

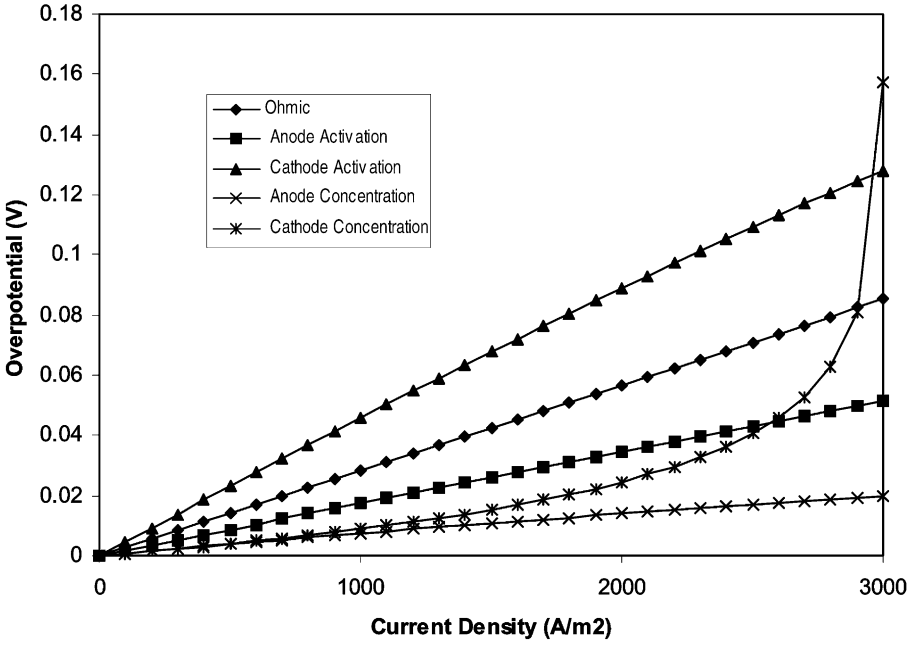

Fig. 4. Detailed contribution of various overpotentials in SOFC at 1073 K.

concentration overpotential becomes significant when the fuel-cell operates near to the limiting current density. Compared with the anode, the cathode exhibits higher activation overpotential, which is due to the poor 'apparent' exchange current density at the electrode/electrolyte (LSM–YSZ/YSZ) interface, as will be seen later in Fig. 8. Since the cathode exchange current density directly affects the electrochemical reaction rate at the cathode, it can be understood that the low electrochemical reaction rate in the cathode leads to high cathode activation polarization in the fuel-cell.

The effect of temperature on the resistance of the anode, cathode, electrolyte and interconnector is presented in Fig. 5a–d, respectively. The resistances of these fuel-cell components are determined by the resistivity of the materials used and their respective thickness. The results show that the resistances of the cathode, electrolyte and interconnector decrease with increase in temperature. By contrast, the anode resistance displays the opposite trend. The resistances of both electrodes are negligible, however, compared with those of the electrolyte and the interconnector, despite the fact that a thick electrode (cathode) was used as the fuel-cell support. The details of the resistivity and thickness of each fuel-cell component are listed in Table 3.

The performance of the fuel-cell as a function of temperature is presented in Fig. 6 in the form of cell voltage versus current density. Results show that the higher the temperature, the lower will be the Nernst potential. As more current is drawn from the fuel-cell, however, a higher cell voltage can be maintained under higher temperature operation at the same current density. There is significant reduction of both Ohmic and activation losses (due to increased exchange current densities) at high temperature operation.

Table 3
Resistivity and thickness of cell components

Material used	Ni–YSZ/YSZ/LSM–YSZ
Anode thickness (μm)	150
Anode Ohmic resistance constant	$a = 0.0000298$, $b = -1392$
Cathode thickness (m)	2E−3
Cathode Ohmic resistance constant	$a = 0.0000811$, $b = 600$
Electrolyte thickness (μm)	40
Electrolyte Ohmic resistance constant	$a = 0.0000294$, $b = 10350$
Interconnect thickness (μm)	100
Interconnect Ohmic resistance constant	$a = 0.001256$, $b = 4690$

This causes an improvement in fuel-cell performance despite the lower Nernst potential at higher temperature.

The effect of temperature on exchange current density is shown in Fig. 7. Both the anodic and cathodic exchange current densities increase exponentially with temperature, which demonstrates the critical dependency of this performance parameter on temperature. The results also clearly indicate that the exchange current density of the anode is more sensitive to the operating temperature than that of the cathode; the difference between the two current exchange densities is about 62% at 1073 K.

The performance of the fuel-cell as a function of operating temperature is presented in Fig. 8 in the form of power density versus current density traces. Results show that the higher the temperature, the higher is the peak power. The location of the peak power shifts towards higher current density as the temperature increases, which shows an improvement in limiting current density at higher temperature. As a compromise between running a fuel-cell at peak power and the stability of operation, it is advisable to operate

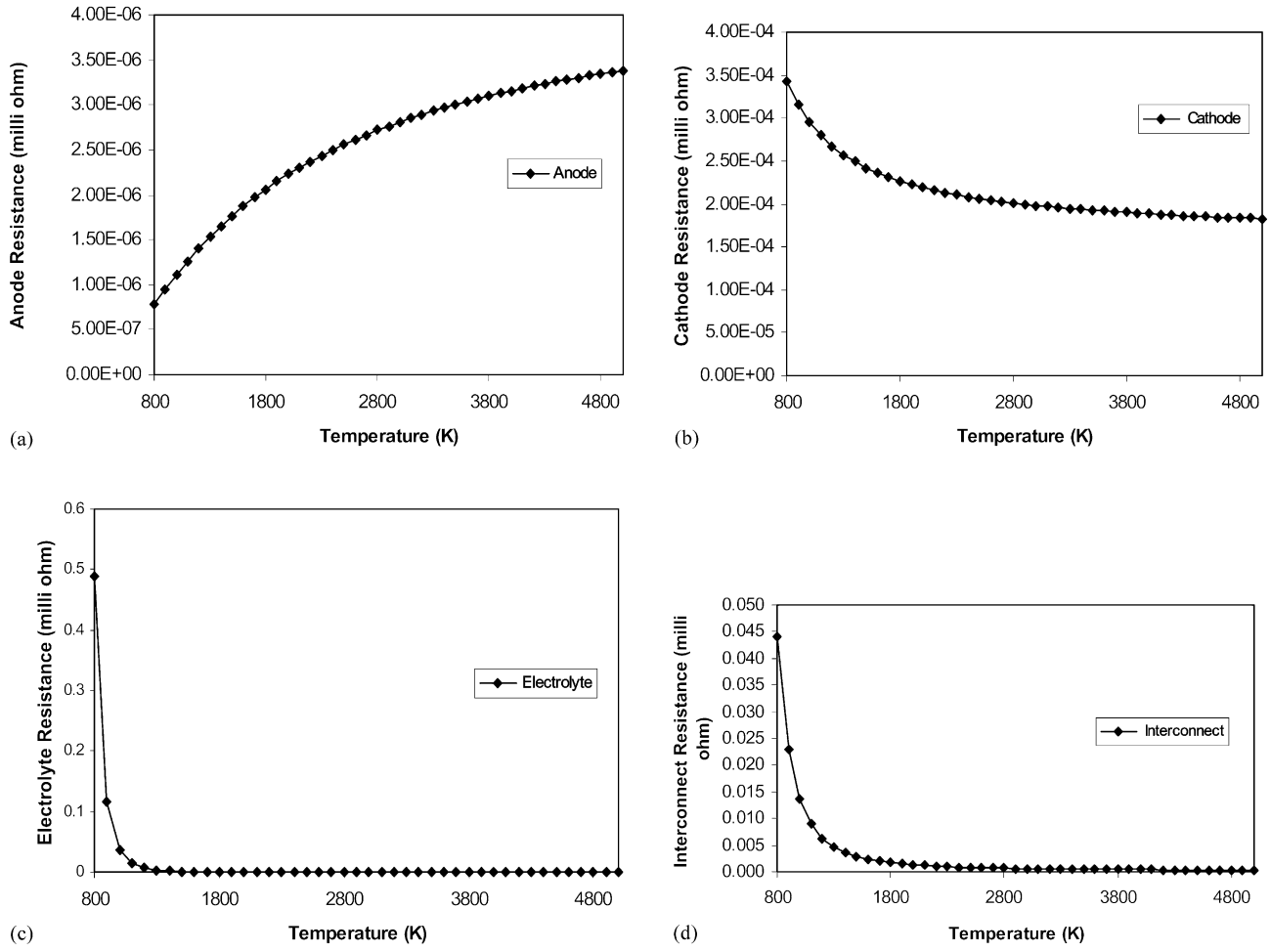

Fig. 5. Effect of temperature on (a) anode Ohmic resistance; (b) cathode Ohmic resistance; (c) electrolyte Ohmic resistance; and (d) interconnector Ohmic resistance.

the SOFC at a current density slightly less than that corresponding to the peak power.

The performance of the fuel-cell, operated between 1073 and 1273 K, is presented in Fig. 9 in the form of maximum power density versus the percentage of current density corresponding to the peak power at the respective limiting current density. Note that the ratio of current density to limiting current density corresponds to the fuel utilization

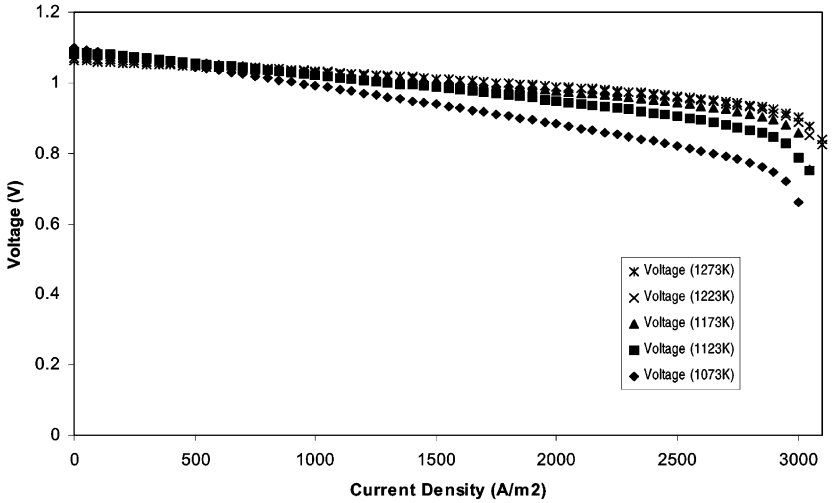

Fig. 6. Effect of temperature of the cell voltage vs. current density trace.

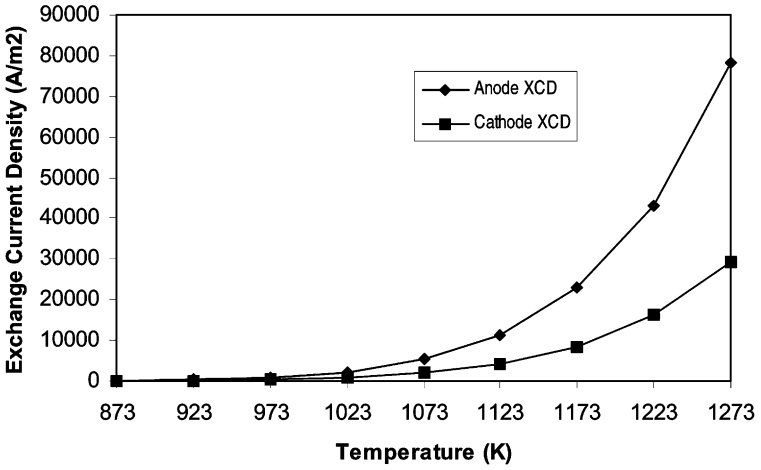

Fig. 7. Effect of temperature on 'apparent' exchange current density.

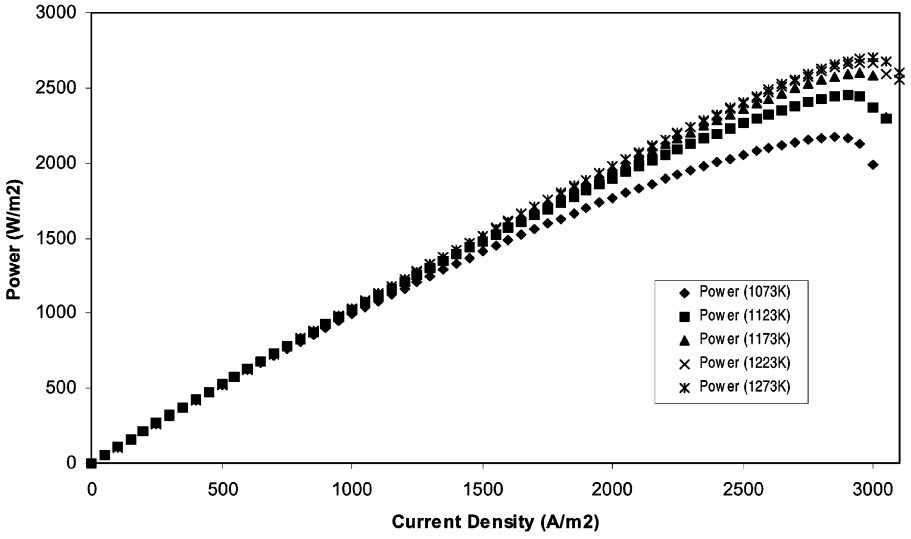

Fig. 8. Effect of temperature on power density.

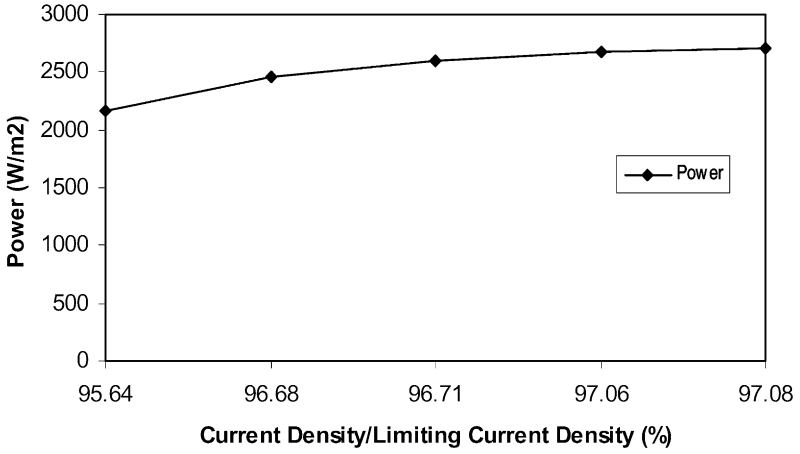

Fig. 9. Peak power density output at respective fuel utilization for temperatures between 1023 and 1273 K.

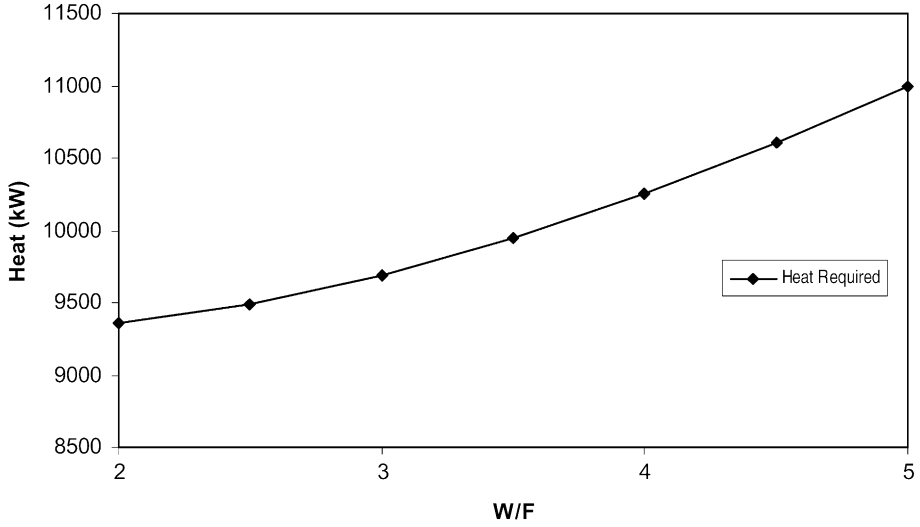

Fig. 10. Effect of molar water/fuel ratio on heat required for reforming (fuel utilization rate: 75%, reformer efficiency: 90%, 973 K (fuel), and 873 K (air)).

rate. The trend for the maximum power is expected to increase with increase in operating temperature, but such a trend is limited by the material constraints and the concentration polarization. As such, it is impossible for the fuel-cell to run at a fuel utilization rate of 100%.

The effect of the amount of water used in the steam reforming on the heat requirement is shown in Fig. 10. The general trend is that the heat required to reform CH_4 gas into H_2 through steam reforming increases with increase in the water/fuel ratio. As mentioned earlier, a molar water/fuel ratio of 2 is sufficient to reform the CH_4, but more water is normally used in order to prevent undesirable formation of carbon due to possible thermal decomposition of the methane. In addition, since the current-reforming model is based only on fixed chemical composition of the product gases and is independent of temperature, no further insight can be gained from this result.

The enthalpy and exergy at each state point of the H_2-fed SOFC system are presented in Fig. 11. In this particular study, the SOFC stack operates at a 75% fuel utilization rate and at 1 atm for both the anode and cathode flow. The fuel and air inlet temperatures of the stack are set to 973 and 873 K, respectively. The performance-related data enthalpy and exergy are, respectively, normalized by the LHV and chemical exergy of H_2. In addition to these data, the temperature at each state point is also shown in Fig. 11. The first value in each control volume is the exergy destruction while the second value is the exergy destruction normalized by the chemical exergy of H_2. Energy transfer through the system boundary of the SOFC stack includes both heat and work transfer. The former, as mentioned earlier, is due mainly to the irreversible electrochemical reaction, while the latter is the output electrical energy of the SOFC stack. Both heat transfer and work transfer are also normalized by the LHV and chemical exergy of H_2, respectively. If a system boundary is drawn to enclose all the control volumes and allow the waste flow energy and heat transfer discharge/dissipate to the environment, it is obvious that the summation of inlet and outlet enthalpies should obey the conservation of energy. In the case of exergy, the input exergies should be balanced by the outlet exergies plus the exergy destructed in all control volumes. Hence, summation of enthalpies at state points 1 and 2 should be equal to enthalpies at state 8 plus the heat dissipated to the environment by the afterburner and SOFC stack and the electrical energy output from the system. Likewise, the summation of exergies at state points 1 and 2 should be equal to the exergy at state 8 plus exergy loss due to heat transfer from the afterburner and SOFC stack, electrical exergy output from the system and the exergies destructed in all control volumes. In the SOFC stack, the normalized values of the electrical work are, respectively, the first law and second efficiencies. In the case of a H_2-fed system, the second law efficiency is higher than the first law efficiency due to the fact that the LHV of H_2 is higher than its corresponding chemical exergy. A study of the system shows that the highest energy lost is due to the heat transfer at the afterburner, which contributes 25.75 and 19.06% of the LHV and chemical exergy of H_2, respectively. It can be explained that, for system of this kind, the isothermal afterburner (i.e. maximum heat loss) is used to prevent excessive increase in the temperatures of H_2 and air at pre-heaters 2 and 1, respectively, so that the SOFC stack can operate within the allowable feedstock temperatures. Note, with too high a feedstock temperature, there will be an adverse effect on the reliability of the stack operation if the stack temperature operates far from its design condition. To improve the overall system efficiency, co-generation may be applied to make use of the waste heat, which is otherwise lost through the cooling system to maintain the isothermal condition of the afterburner. In view of the low exergy destruction in all control volumes, an improvement of thermal efficiency can be obtained by operating the stack at high fuel utilization, but not excessively high to cause problems of severe

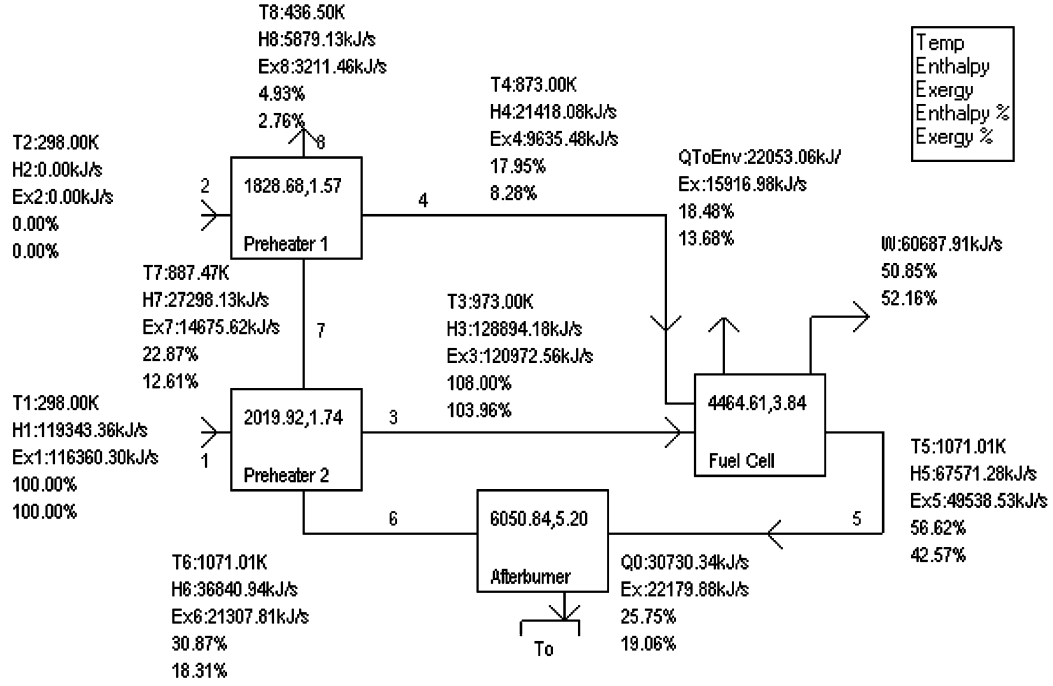

Fig. 11. Hydrogen-fed system operating at 75% fuel utilization, 1 atm (anode and cathode), 973 K (fuel), and 873 K (air).

concentration overpotential and overheating at high stack temperatures.

Slightly more complicated system is shown in Fig. 12 and consists of a vaporizer, a mixer and a reformer in addition to the basic system requirements described above. To provide a comparison with a H_2-fed system, all performance-related input parameters are set to the same values. Results show that the first and second law efficiencies of this CH_4-fed SOFC system are 62.19 and 59.96%, respectively, which are higher than those in a H_2-fed system. Note, the first law

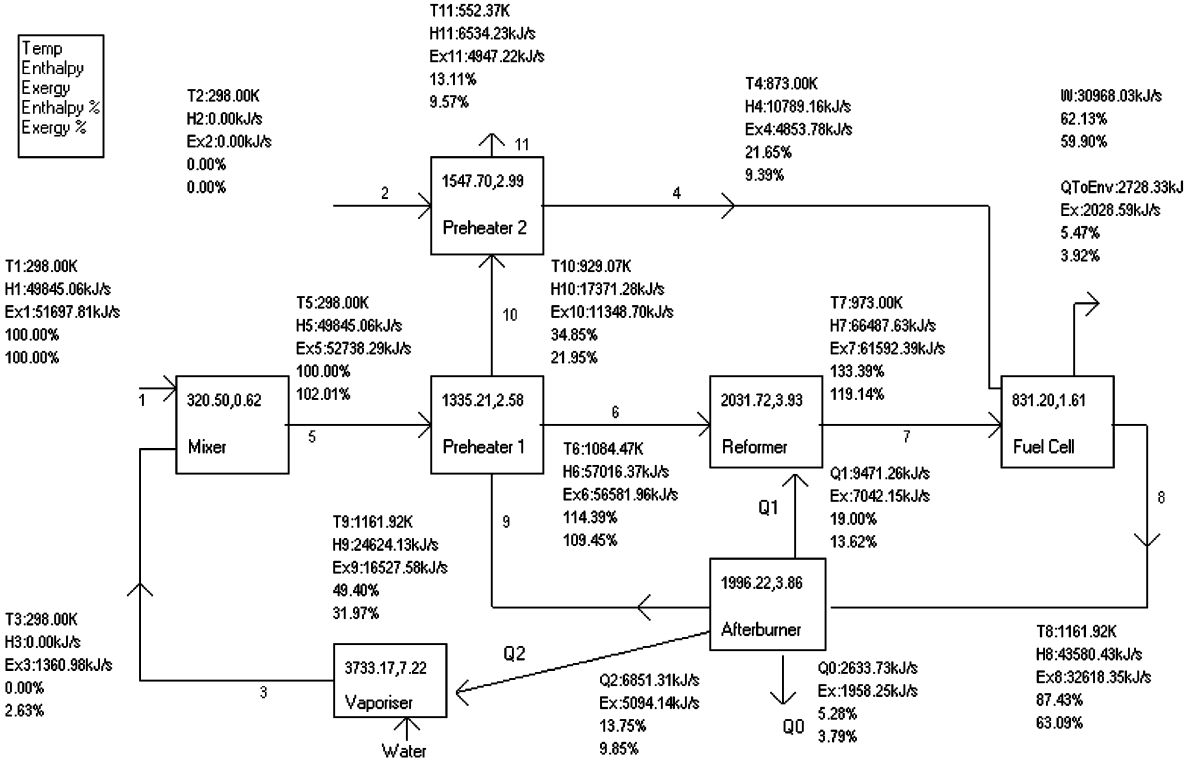

Fig. 12. Methane-fed system operating at 75% fuel utilization, 1 atm (anode and cathode), 973 K (fuel), and 873 K (air).

efficiency, in this case, is higher than the second law efficiency and is attributed to the fact that the chemical exergy of the fuel is higher than its corresponding LHV. In this system, all losses (exergy destruction in all control volumes, heat transfer and flow exergy leaving the system) are rather well distributed with higher flow exergy loss at the exit of pre-heater 1 (9.57%) and exergy destruction in the vaporizer (7.22%). Compared with a H_2-fed system, the heat transfer loss to the environment in a CH_4-fed system is lower. This is attributed to a higher demand for heat energy used by the reformer and vaporizer.

5. Conclusions

A simulation program has been developed to simulate two simple SOFC power systems which use hydrogen and methane as the feedstock fuels. Based on this study, the following conclusions are made.

- The fuel-cell model developed in this study can replicate well the characteristics of the fuel-cell under different operating conditions, as well as and the electrical properties of the materials used in the cell components. The parameters related to electrochemical processes and transport phenomena are all expressed as the function of thermodynamic state.
- The fuel-cell model can be used to simulate different designs of SOFC provided that the geometric specifications, performance-related parameters and operating conditions are specified.
- In a simple SOFC power system with only waste heat recovery used for pre-heating the fuel and air, the system efficiency can be improved by operating the fuel-cell stack at a high fuel utilization rate, but not excessively high to cause problems of concentration overpotential or overheated cells due to high stack temperature associated with high cell polarization.
- At a 75% fuel utilization rate, 1 atm of anode and cathode flow pressure, a 973 K of fuel inlet temperature of 973 K and an air inlet temperature of 873 K, simulated results showed that a H_2-fed system can achieve 50.97 and 52.28% of the first and second law efficiencies, respectively. For a CH_4-fed system under the same settings, the corresponding first and second law efficiencies are, respectively, 62.19 and 59.96%.

References

[1] S.E. Veyo, W.L. Lundberg, Solid-oxide fuel-cell power system cycles, ASME Paper 99-GT-356, 1999.
[2] G.T. Lee, F.A. Sudhoff, Fuel-Cell/Gas-Turbine System Performance Studies, Fuel-Cells 1996 Review Meeting, FETC Publications, Dept. of Energy, USA, 1996.
[3] P.F. van den Oosterkamp, A.A. Goorse, L.J.M.J. Blomen, J. Power Sources 41 (1993) 239–252.
[4] K.W. Bedringas, I.S. Ertesvag, S. Byggstoyl, B.F. Magnussen, Energy 22 (4) (1997) 403–412.
[5] R.L. Cornelissen, Thermodynamics and sustainable development — the use of exergy analysis and the reduction of irreversibility, Ph.D. thesis, Universiteit Twente, The Netherlands, 1997.
[6] S. Gordon, B.J. McBride, NASA SP-273, USA, 1971.
[7] N.F. Bessette II, W.J. Wepfer, J. Winnick, J. Electrochem. Soc. 142 (1995).
[8] S.H. Chan, K.A. Khor, Z.T. Xia, J. Power Sources 93 (2001) 130–140.
[9] A.L. Hines, R.N. Maddox, Mass Transfer: Fundamentals and Applications, Prentice-Hall, Englewood Cliffs, NJ, 1985.
[10] C.J. Geankoplis, Mass Transport Phenomena, Holt, Rinehart and Winston, New York, 1972.
[11] F.P. Incropera, D.P. Dewitt, Fundamentals of Heat and Mass Transfer, 4th Edition, Wiley, New York, 1996.